Vibrational Spectroscopy 64 (2013) 1–9

Contents lists available at SciVerse ScienceDirect

Vibrational Spectroscopy

journal homepage: www.elsevier.com/locate/vibspec

Interpretation of the IR and Raman spectra of morin by density functional theory and comparative analysis

Jasmina M. Dimitrić Marković[a,*], Zoran S. Marković[b], Jugoslav B. Krstić[c], Dejan Milenković[d], Bono Lučić[e], Dragan Amić[f]

[a] Faculty of Physical Chemistry, University of Belgrade, Studentski trg 12-16, 11000 Belgrade, Serbia
[b] Department of Biochemical and Medical Sciences, State University of Novi Pazar, Vuka Karadžića bb, Novi Pazar 36300, Serbia
[c] Institute of Chemisty, Technology and Metallurgy – Department of Catalysis and Chemical Engineering, Njegoševa 12, 11000 Belgrade, Serbia
[d] Bioengineering Research and Development Center, 34000 Kragujevac, Serbia
[e] NMR Center, Rudjer Bošković Institute, P.O. Box 180, HR-10002 Zagreb, Croatia
[f] Faculty of Agriculture, The Josip Juraj Strossmayer University, P.O. Box 719, HR-31107 Osijek, Croatia

ARTICLE INFO

Article history:
Received 27 March 2012
Received in revised form 24 October 2012
Accepted 24 October 2012
Available online 2 November 2012

Keywords:
Morin
Quercetin
IR and Raman spectra
Comparative analysis
M05-2X-6-311++G(d,p)

ABSTRACT

Density functional theory calculations, with M05-2X functional and 6-311++G(d,p) basis set implemented in the Gaussian 09 package, are performed with the aim to support molecular structure and spectroscopic characteristics of morin, a bioflavonoid molecule known for its antiproliferative, antitumor, and anti-inflammatory effects. Detailed vibrational spectral analysis and the assignments of the bands, done on the best-fit basis comparison of the experimentally obtained and theoretically calculated IR and Raman spectra, match quite well indicating DFT calculations as very accurate source of normal mode assignments. The assignment of the most prominent normal modes of morin is qualitatively verified through comparative spectral analysis with quercetin, a structurally isomeric molecule of morin which differs only by the substitution pattern of the B ring. Performed comparative analysis reflects quite accurately all the structural differences between the investigated molecules additionally proving the applied theoretical method.

1. Introduction

Health human body maintains a delicate balance between antioxidants and oxidants. When that status is disrupted oxidative stress prevails causing oxidative damage of biologically important molecules (DNA, amino acids, proteins) which is implicated in aging process and neurodegenerative diseases (such as Alzheimer's and Parkinson's) [1–5], cancer [6,7] or cardiovascular diseases such as hypertension, arteriosclerosis, heart attack or stroke [8–10]. Flavonoids are natural phenolic compounds recognized as potent external defense factors against oxidative damage. Among very diverse activities the most interest has been focused to their antioxidant activity which act via different mechanisms like direct free radical scavenging, modulation of cell signaling, chelation of transition metal ions, inhibition of certain enzymes (lipase, telomerase, pepsin, trypsin, α-amylase) or removing oxidatively changed and damaged biomolecules [11–21].

Morin is pentahydroxy flavone isolated as yellow pigment from almond hulls, old fustic (*Chlorophora tinctoria*) and members of the Moraceae family, such as mulberry, figs and other Chinese herbs. Although its biological effects are not fully understood there are some circumstantial evidence that morin has the ability to: suppress the proliferation of a wide variety of tumor cells [18–20], inhibit lipooxygenase-1 [22], induces differentiation of keratinocytes [20], inhibit P-glycoprotein [23] or reduce the incidence of lipopolysaccharide (LPS)-induced septic shock [12]. All these effects rank morin as highly biologically potent and active flavonoid.

The present study comprises in vitro experimental (Raman) and theoretical approaches in analysis of morin structure. To our knowledge, no attempts to theoretically assign the experimental vibrational spectra of morin have been done yet. Nowadays, the progress of various theoretical methods has made possible the calculation of vibrational potential fields of medium size molecules with moderate computational effort. In particular, density functional methods such as M052X, which showed an excellent performance for planar organic molecules [24], is used to predict vibrational frequencies of morin.

2. Experimental

2.1. Computational methods

The structure of morin was fully optimized with a new local density functional method (M05-2X) that was developed by Truhlar

* Corresponding author. Tel.: +381 11 33366 24; fax: +381 11 2187 133.
E-mail address: markovich@ffh.bg.ac.rs (J.M. Dimitrić Marković).

0924-2031/$ – see front matter © 2012 Elsevier B.V. All rights reserved.
http://dx.doi.org/10.1016/j.vibspec.2012.10.006

Table 1
Geometrical parameters of the absolute minimum of morin calculated by M05-2X method with 6-311++G(d,p) basis set.

Bond lengths (Å)	Exp. values[a]	Calculated	Angles (°)	Exp. values	Calculated
C(2)—O(1)	1.375	1.364	O(l)—C(2)—C(3)	120.4	119.6
C(2)—C(3)	1.355	1.353	O(l)—C(2)—C(1′)	111.2	112.15
C(2)—C(1′)	1.464	1.462	C(3)—C(2)—C(l′)	128.3	128.2
C(3)—C(4)	1.455	1.444	C(2)—C(3)—C(4)	121.9	122.2
C(3)—O(3)	1.372	1.363	C(2)—C(3)—O(3)	120.2	122.5
C(4)—C(10)	1.438	1.433	C(4)—C(3)—O(3)	117.7	115.3
C(4)—O(4)	1.258	1.244	C(3)—C(4)—C(10)	115.6	115.9
C(10)—C(5)	1.425	1.415	C(3)—C(4)—O(4)	120.1	119.1
C(10)—C(9)	1.396	1.400	C(10)—C(4)—O(4)	124.3	124.9
C(5)—C(6)	1.368	1.382	C(4)—C(10)—C(5)	122.3	121.9
C(5)—O(5)	1.348	1.335	C(4)—C(10)—C(9)	119.9	122.2
C(6)—C(7)	1.410	1.397	C(5)—C(10)—C(9)	117.8	118.7
C(7)—C(8)	1.396	1.389	C(10)—C(5)—C(6)	120.3	119.8
C(7)—O(7)	1.349	1.352	C(10)—C(5)—O(5)	120.0	120.8
C(8)—C(9)	1.386	1.383	C(6)—C(5)—O(5)	119.6	119.4
C(9)—O(1)	1.369	1.356	C(5)—C(6)—C(7)	119.9	119.4
C(l′)—C(2′)	1.404	1.406	C(6)—C(7)—C(8)	121.6	122.3
C(2′)—C(3′)	1.394	1.393	C(6)—C(7)—O(7)	117.1	121.1
C(2′)—O(2′)	1.370	1.349	C(8)—C(7)—O(7)	121.3	116.6
C(3′)—C(4′)	1.376	1.384	C(7)—C(8)—C(9)	117.1	117.5
C(4′)—C(5′)	1.394	1.396	0(l)—C(9)—C(10)	121.2	120.7
C(4′)—0(4′)	1.372	1.357	O(l)—C(9)—C(8)	115.5	117.0
C(5′)—C(6′)	1.378	1.375	C(10)—C(9)—C(8)	123.3	122.2
C(l′)—C(6′)	1.403	1.405	C(2)—C(l′)—C(2′)	123.9	124.0
O(2′)—H(2′)	1.000	0.970	C(2)—C(l′)—C(6′)	118.5	117.9
O(4′)—H(4′)	0.913	0.959	C(l′)—C(2′)—C(3′)	120.6	119.8
O(3)—H(3)	0.845	0.973	C(l′)—C(2′)—O(2′)	122.5	124.4
O(5)—H(5)	0.912	0.979	C(3′)—C(2′)—0(2′)	116.8	115.8
O(7)—H(7)	0.877	0.960	C(2′)—C(3′)—C(4′)	120.1	120.6
O(2′)—H(2′)···O(3)	1.739	1.747	C(3′)—C(4′)—C(5′)	120.6	120.5
O(3)—H(3)···O(4)	2.287	2.052	C(3′)—C(4′)—O(4′)	122.0	122.2
O(5)—H(5)···O(4)	1.832	1.788	C(5′)—C(4′)—O(4′)	117.3	117.3
			C(4′)—C(5′)—C(6′)	119.00	118.71
			C(l′)—C(6′)—C(5′)	122.10	122.29
			C(2)—O(l)—C(9)	120.80	122.07
			Torsion angles		
			t(C(3)—C(2)—C(1′)—C(2′))	−43.40	38.50

[a] Crystallographic measurements in (Å) [38].

group [25] using the 6-311++G(d,p) basis set, as implemented in the Gaussian 09 package [26]. This new hybrid meta exchange correlation functional is parameterized so that it includes both nonmetallic and metallic compounds. This functional also yields satisfactory overall performance for main-group thermochemistry and thermochemical kinetics, as well as for organic, organometallic, biological and noncovalent interactions [25,27,28]. The vibrational frequencies were obtained by diagonalizing the corresponding M05-2X Hessian matrices. The nature of the stationary points was determined by analyzing the number of imaginary frequencies: 0 for a minimum and one imaginary for a transition state. Relative energies were calculated at 298 K.

The vibrational modes were assigned on the basis of PED analysis using VEDA 4 program [29] with its visualization interface. Normal coordinate analysis of morin was carried out in order to link theoretical models to experimentally accessible data much easier, thus enabling straightforward interpretation of molecular events. The calculated vibrational wavenumbers were scaled with the uniform scaling factor of 0.9444 [30–33] in order to get better match between calculated and experimental wavenumber values.

Potential energy surfaces were obtained in relation with the torsion angle between rings B and C, defined by the C3—C2—C1′—C2′ atoms. The torsion angle τ was scanned in steps of 15° without constraints on all other geometrical parameters. The effects of the following torsion angles rotations were also studied: C10—C5—OH, C6—C7—OH, C2—C3—OH, C3′—C2′—OH, and C5′—C4′—OH. Afterwards, the structures were further optimized without any constraint around each potential minimum. The natural bond orbital (NBO) analysis [34–36] of morin was also performed.

2.2. Raman spectra

Raman spectra were recorded on Thermo Scientific Nicolet Almega XR Raman spectrometer equipped with an Olympus optical microscope and a CCD detector. The spectra were excited with a diode pumped solid state high-brightness 532 nm laser. Objective lens was 50×. The scattered light was analyzed by the spectrograph with a 900 lines/mm grating. The spectra were obtained in the region 3500–400 cm^{-1} directly from the pure powder samples. The laser output was kept at 10 mW. Acquisition time was 10 s with 10 scans. The fluorescence correction has been done. Thermo Scientific OMNIC software was used for data acquisition and data processing.

The theoretical Raman intensities (I_i^R) were derived from the computed Raman scattering activities using the following equations:

$$I_i^R = C(\upsilon_0 - \upsilon_i)^4 \cdot \upsilon_i^{-1} \cdot B_i^{-1} \cdot S_i \quad (1)$$

where B_i is a temperature factor which accounts for the intensity contribution of excited vibrational states, and is represented by the Boltzmann distribution:

$$B_i = 1 - \exp\left(-\frac{h\upsilon_i c}{kT}\right) \quad (2)$$

In Eq. (1), υ_0 is the wavenumber of the laser excitation line (υ_0 = 18,797 cm^{-1} which corresponds to the wavelength of 532 nm), υ_i is the wavenumber of normal mode (cm^{-1}), while S_i is the Raman scattering activity of the normal mode Q_i. The theoretical Raman intensity, I_i^R, is given in arbitrary units (C is a constant equal to 10^{-12}). In Eq. (2) h, k, c, and T are Planck and Boltzmann constants, speed of light and temperature in Kelvin, respectively.

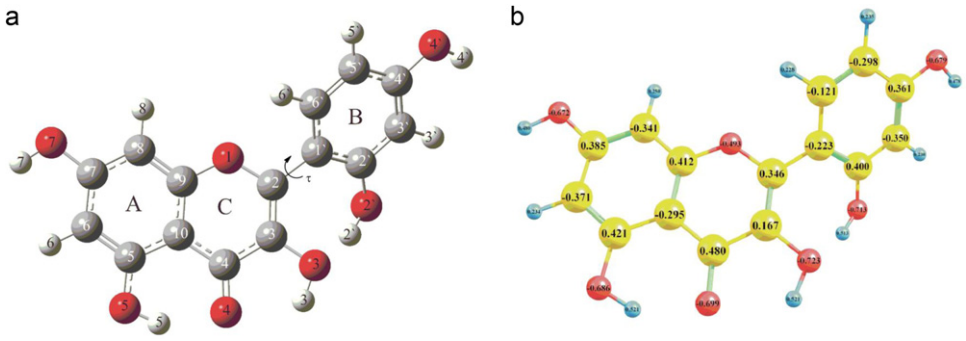

Fig. 1. Structure and atomic numbering of morin (a) and natural charge distribution of morin (b).

The value of factor B_i was assumed to be 1. Otherwise, as reported in the literature [37], the calculated Raman intensities for the bands below 300 cm^{-1} were extremely overestimated in comparison to the experiment.

2.3. IR spectra

IR spectra were recorded on a Thermo Nicolet 6700 FT-IR Spectrometers with ATR and DTGS TEC detector. The spectra were recorded in the middle IR region, 4000–400 cm^{-1}. The spectral resolution was 2 cm^{-1}, the number of samples scans 512, the number of background scans 512. Morin (Merck, USA) was studied in potassium bromide matrix with a ratio of (1:200) mg (morin:KBr).

3. Results and discussion

3.1. Geometry of morin

The obtained geometrical parameters of morin (bond lengths, bond angles, and torsional angles), calculated by using M05-2X/6-311++G(d,p) level of theory, are presented in Table 1. In order to determine the preferred relative positions between the rings B and C, rotational barrier (Fig. 1a), and relative stabilities of isomers, conformational analysis was performed as a function of torsional angle between those rings. It is found that morin has a non planar geometry with the part of the molecule, containing cycles A and C, which has complete planarity. The calculated value of 38.5° (for the most stable conformation of morin, see Table 1) is in good agreement with experimental value of 43.4° [38]. In order to examine potential energy surface, the torsion angle τ was scanned in steps of 15° without constraints on all other geometrical parameters. Removing constrain for the torsional angle τ the conformational absolute minimum is found at $\tau = 38.52°$, followed by a relative minimum at $\tau = 149.35°$. All stationary and transition states points are reoptimized, in further discussion free energies values are used. The energy difference between these two minima is 2.3 kcal mol^{-1}. The maximum of the potential energy lies at $\tau = 92°$ and the introversion barrier between the two minima is about 6.2 kcal mol^{-1}. There is also another maximum at 0°, with energy of 3.5 kcal mol^{-1} which indicates that both minima at $\tau = -38.52°$ and $\tau = 38.52°$ are in equilibrium at room temperature (Fig. 2). All the hydroxyl groups in the molecule of morin are oriented in a way to form the maximum number of internal hydrogen bonds (IHB), which is three (Fig. 1a). Two IHBs are formed between C4—O carbonyl group and C3-OH and C5—OH groups and the third one is formed between C2′—OH and C3—OH groups. The conformations lacking these bonds are less stable with respect to the absolute minimum [39], which means that the IHBs have an additional stabilizing effect on morin structure.

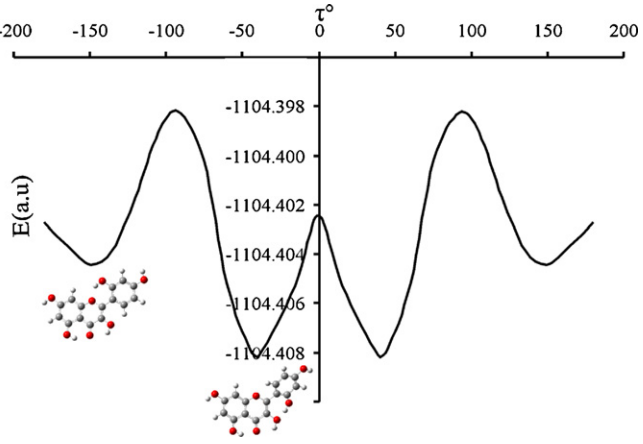

Fig. 2. A plot of the potential energy scan as a function of angle τ.

3.2. NBO analysis

The natural bond orbital (NBO) analysis provides a description of the conformer structure by a set of localized bonds, antibonds and Rydberg extravalence orbitals. The destabilizing interactions between occupied orbitals and stabilizing interactions between occupied and unoccupied orbitals can be obtained from this analysis [36,40–42]. The various second order interactions, between the occupied orbitals of one subsystem and vacant orbitals of another subsystem, as a measure of the delocalization or hyperconjugation [43], are calculated using M05-2X/6-311++G** level of theory. The hyperconjugative interaction energy was deduced from the second-order perturbation approach as:

$$E(2) = -n_\sigma \frac{\langle \sigma|F|\sigma\rangle^2}{\varepsilon_{\sigma^*} - \varepsilon_\sigma} = -n_\sigma \frac{F_{ij}^2}{\Delta E} \quad (3)$$

where $\langle \sigma|F|\sigma\rangle^2$, or F_{ij}^2 is the Fock matrix element [44] between i and j NBO orbitals, ε_σ and ε_{σ^*} are the energies of σ and σ^* NBO's, and n_σ is the population of the donor σ orbital. The main natural orbital interactions were analyzed with the NBO 5.9 program [45].

It is well known that the NBO analysis is an efficient method for investigating hyperconjugative interaction or charge transfer (CT) in molecular systems. Some electron donor orbital, acceptor orbital and the interacting stabilization energies resulting from the second-order micro disturbance theory have been already reported [46]. It should be noted that the higher value of $E(2)$ represents the more intensive interaction between electron donors and electron acceptors. The second-order perturbation theory analysis of Fock matrix in the NBO basis of the molecule shows strong intramolecular hyperconjugative interactions which are in presented Table S1 (Supplementary Information). The electron

Table 2
Experimental and calculated positions of the bands in IR and Raman spectra of morin, assignments and intensities[a] of the normal modes (scaling factor 0.9444).

Mode	Assignment	ν_{IR} exp. (cm^{-1})	ν_{R} exp. (cm^{-1})	M05-2X/6-311++G(d,p)				
				ν_{scaled} (cm^{-1})	IR intensity	Raman intensity	Raman activity ($Å^4$ amu^{-1})	PED (%)
90	OH stretching (A) (C4′—OH)	3565		3632.3	0.39	2.8	21.3	ν_{OH} (100)
89	OH stretching (A) (C7—OH)	3508		3611.4	0.30	3.5	24.6	ν_{OH} (100)
88	OH stretching (C) (C3—OH)	3384 sh		3580.2	0.36	1.8	36.8	ν_{OH} (100)
87	OH stretching (C, B) (C5—OH)	3311		3313.5	0.50	2.3	21.8	ν_{OH} (99)
86	OH stretching (A) (C2′—OH)	3244		3150.8	0.00	4.1	20.9	ν_{OH} (99)
85	CH stretching (A)	3101		3056.4	0.10	3.0	18.8	ν_{CH} (100)
84	CH stretching (B)	2961 sh		2991.2	0.10	5.3	31.2	ν_{CH} (99)
83	CH stretching (B)	2850 sh		2897.8	0.00	1.8	10.3	ν_{CH} (100)
82	CH stretching (A)	2783 sh		2776.6	0.00	2.3	35.3	ν_{CH} (99)
81	CH stretching (B)	2632 sh		2566.1	0.00	3.0	48.9	ν_{CH} (99)
80	CC stretching (C) (C2=C3) OC stretching (A, C) (C3—O, C5—O)	1658 vs	1667 s	1663.6	0.46	100.0	812.4	ν_{CC} (56)
79	CC stretching (C) (C2=C3) CO stretching (C) (C=O)	1632 vs	1626 vs	1636.5	0.60	77.8	199.3	ν_{CC} (51)
78	CC stretching (B)			1616.6	1.00	25.5	225.3	ν_{CC} (49) + δ_{HCC} (10)
77	C=O stretching (C) CC stretching (C) (C2=C3, C9—C10) CC stretching (A)	1597 vs		1596.4	0.18	19.4	155.9	ν_{OC} (56)
76	OC stretching (A, C) (C=O, C3—O, C5—O) CC stretching (A, B, C) (C2=C3)	1574 s	1579 s	1580.4	0.17	63.8	336.7	ν_{CC} (29) + δ_{CCC} (10)
75	OC stretching (C) (C=O) COH bending (B) (C5—OH)		1544 vw	1558.1	0.01	2.3	13.6	ν_{OC} (58)
74	OC stretching (C) (C=O) CCC bending (B) (C2′—C3′—C4′) HCC bending (B) (H3′—C3′—C4′)	1503 s	1501 m	1497.4	0.41	26.4	145.3	δ_{HCC} (29) + δ_{CCC} (11)
73	CC stretching (A) OC stretching (A) CCO bending (A, C)	1489 sh		1484.6	0.01	6.3	39.8	ν_{CC} (11) + δ_{CCO} (12)
72	CC stretching (B) COH bending (A, C) (C3—OH, C5—OH, C7—OH) CCC bending (A)	1461 m	1468 w	1467.6	0.32	10.6	59.9	ν_{OC} (12) + δ_{COH} (12) + δ_{CCC} (12)
71	COH bending (C, A) (C3—OH, C5—OH) CC stretching (A)		1430 w	1432.2	0.07	41.1	264.7	ν_{CC} (28) + ν_{OC} (13)
70	CC stretching (A) CCO bending (A, C)	1418 m	1398 vw	1405.4	0.00	1.3	6.5	ν_{CC} (10) + δ_{CCO} (14)
69	CC stretching (A) COH bending (B) (C4′—OH)	1377 s	1368 m	1362.0	0.32	21.9	135.5	ν_{CC} (47) + δ_{COH} (28)
68	OC stretching (A, C)			1347.5	0.21	12.8	87.3	ν_{CC} (11) + ν_{OC} (43)
67	COH bending (C) (C3—OH) CC stretching (B)	1332 m	1332 m	1326.6	0.00	37.8	231.1	ν_{CC} (31) + δ_{COH} (26)
66	OC stretching (B) COH bending (B) (C2′—OH, C4′—OH) CCH bending (B)		1302 w	1310.4	0.16	8.5	66.3	ν_{CC} (13) + δ_{COH} (18) + δ_{HCC} (11)

Table 2 (*Continued*)

Mode	Assignment	ν_{IR} exp. (cm^{-1})	ν_{R} exp. (cm^{-1})	M05-2X/6-311++G(d,p)				
				ν_{scaled} (cm^{-1})	IR intensity	Raman intensity	Raman activity ($Å^4$ amu^{-1})	PED (%)
65	OC stretching (A) (C5—O) COH bending (A, B, C) CCH bending (A, B)	1291 s		1287.1	0.20	26.1	188.3	ν_{CC} (13) + δ_{COH} (14) + δ_{HCC} (11)
64	CC stretching (C, B) COH bending (C) (C3—OH)	1261 s		1273.0	0.52	10.3	71.3	ν_{CC} (23) + δ_{COH} (31)
63	CC stretching (C, B) OC stretching (C, B) COH bending (B) (C2′—OH, C4′—OH)	1243 s	1242 w	1242.9	0.19	0.3	1.1	ν_{CC} (26) + ν_{OC} (10) + δ_{COH} (13)
62	OC stretching (C) COH bending (A, C) (B) (C3—OH, C5—OH)			1228.5	0.00	4.7	24.1	δ_{COH} (22)
61	OC stretching (B) (C2′—O) OC stretching (A, C) (C3—O, C5—O) HCC bending (B)	1215 m	1213 w	1217.8	0.00	0.2	41.1	δ_{HCC} (34)
60	CC stretching (C–B) COH bending (A, C) HCC bending (A)	1191 m		1183.5	0.56	2.0	12.2	ν_{CC} (10) + δ_{COH} (36) + δ_{HCC} (17)
59	CCO bending (C)	1161 vs		1160.4	0.24	0.05	1.9	ν_{OC} (47)
58	HCC bending (B) COH bending (B) (C4′—OH) CCC bending (C)		1158 vw	1147.6	0.00	5.3	28.7	ν_{OC} (35) + δ_{COH} (20) + δ_{HCC} (20)
57	CCC bending (B)	1137 m		1139.4	0.42	0.02	1.6	ν_{OC} (21) + δ_{HCC} (25)
56	COH bending (B) (C2′—OH)		1131 vw	1128.7	0.05	0.06	0.02	δ_{COH} (42) + δ_{HCC} (23)
55	COH bending (A)			1119.8	0.05	0.07	0.03	δ_{COH} (30) + δ_{HCC} (31)
54	COH bending (C)	1100 w	1096 vw	1101.1	0.01	2.9	15.3	δ_{COH} (27)
53	COH bending (A)	1081 m		1077.6	0.01	0.09	0.1	ν_{OC} (25)
52	COH bending (A, B, C)		1060 vw	1068.9	0.01	0.08	0.08	δ_{CCC} (12)
51	HCC bending (A, B)	979 w	1007 vw	1005.0	0.01	0.06	0.02	δ_{HCC} (24)
50	HCC bending (B) (H5′—C5′—C4′) CCC bending (B) (C2′—C3′—C4′)	967 w	981 w	977.9	0.01	5.6	30.2	ν_{CC} (32) + ν_{OC} (10) + γ_{HCCC} (11) + δ_{CCC} (12)
49	HCC bending (A, B, C)			963.3	0.05	5.7	27.8	ν_{OC} (10) + ν_{CC} (19) + γ_{HCCC} (15)
48	HCC bending (A, B)	881 w	939 vw	946.7	0.06	0.8	1.0	δ_{HCC} (10) + γ_{HCCC} (72) + τ_{CCCC} (15)
47	HCC bending (B) (H3′-C3′-C2′)	852 w	876 w	876.4	0.10	1.9	11.6	δ_{CCO} (26) + γ_{HCCC} (15)
46	CCO bending (C) COC bending (C)	839 w	813 vw	817.5	0.10	1.1	1.7	δ_{CCO} (53) + τ_{CCCC} (12) + γ_{OCCC} (12) + γ_{HCCC} (11)
45	CCC bending (B)	825 w	795 vw	790.9	0.00	0.1	0.4	τ_{HCCC} (81) + τ_{OCCC} (10)
44	CCO bending (A–C)			787.3	0.01	0.07	0.6	τ_{HCCC} (65)
43	CCC bending (B) (C2′—C1′—C6′)			785.8	0.00	0.9	3.9	δ_{CCC} (53) + τ_{CCCC} (11) + τ_{OCCC} (19)
42	CCC bending (B) (C3′—C4′—C5′)	793 m	789 vw	783.7	0.00	0.9	4.2	ν_{OC} (73)
41	CCC bending (B) (C2′—C3′—C4′)		763 vw	759.6	0.00	0.6	0.3	δ_{CCC} (24) + γ_{OCCC} (43)
40	CCO bending (A–C)		748 vw	750.2	0.10	5.8	30.5	δ_{CCO} (19) + δ_{CCC} (12)
39	CCC bending (A)		735 vw	730.3	0.00	0.6	2.1	τ_{HOCC} (52)
38	CCO bending (A, B)		710 vw	723.3	0.00	1.7	7.6	ν_{OC} (11) + δ_{CCO} (11) + τ_{OCCC} (10)
37	CCC bending (A, B, C)	699 vw		718.9	0.01	1.2	5.9	δ_{CCC} (21)
36	CCO bending (B)	685 vw	688 vw	679.4	0.00	1.1	4.8	τ_{HCCC} (15) + τ_{OCCC} (16) + γ_{CCOC} (19)

Table 2 (*Continued*)

Mode	Assignment	ν_{IR} exp. (cm^{-1})	ν_R exp. (cm^{-1})	M05-2X/6-311++G(d,p)				
				ν_{scaled} (cm^{-1})	IR intensity	Raman intensity	Raman activity ($Å^4$ amu^{-1})	PED (%)
35	CCO bending (A, B)	662 vw		657.7	0.00	1.6	3.2	δ_{CCO} (14) + τ_{CCOC} (13)
34	CCO bending (B)		654 w	646.2	0.00	4.4	15.5	τ_{OCCC} (26)
33	CCO bending (C) COC bending (C)	638 vw	638 w	631.1	0.00	1.0	5.6	δ_{CCO} (17) + τ_{HCCC} (11) + γ_{OCCC} (29)
32	CCC bending (C–B)	619 vw		616.0	0.01	1.4	4.8	τ_{CCOC} (31) + γ_{CCOC} (10)
31	CCO bending (C)			603.5	0.00	2.7	7.6	δ_{CCO} (12)+ τ_{HOCC} (72)
30	CCO bending (A–C) CCC bending (C–B)	602 vw	605 vw	600.9	0.00	2.9	5.6	δ_{CCO} (13) + τ_{HCCC} (10) + γ_{OCCC} (25)
29	CCOH torsion (B)			591.1	0.00	3.1	9.9	τ_{HOCC} (33)
28	CCOH torsion (B)	583 vw	580 m	587.4	0.10	3.6	12.2	τ_{HOCC} (33)
27	CCOH torsion (C)	565 vw	568 vw	574.6	0.00	3.6	13.6	δ_{CCC} (12) + δ_{CCO} (23)
26	CCOH torsion (C)			557.7	0.00	1.9	5.1	ν_{CC} (11) + ν_{OC} (11) + δ_{CCC} (31)
25	CCOH torsion (B, C)		547 vw	555.3	0.00	1.4	3.2	δ_{CCC} (10) + δ_{CCO} (26) + τ_{CCOH} (19)
24	CCCH torsion (A)		522 vw	519.0	0.00	1.1	2.9	δ_{CCO} (41) + τ_{CCCH} (28)
23	CCCH torsion (A)			493.3	0.00	0.9	2.8	τ_{CCCH} (14) + τ_{OCCC} (23)
22	CCCH torsion (B)	489 vw		477.8	0.00	0.9	1.1	τ_{CCCH} (25) + δ_{CCO} (10)

Raman intensities are calculated using the formulae for Raman intensity and after that are normalized to 100; Raman activity = S_i of the normal mode.
ν – stretching modes; δ – bending modes; τ – torsional modes; γ – out of plane modes; sh – shoulder; vw – very weak; w – weak; m – medium; s – strong; vs – very strong.
[a] IR intensities are normalized with highest peak equal to 1.

donation from the lone pair (LP2) O atoms of the electron donating groups to the π^*(C—C) anti-bonding acceptor orbital of the phenyl ring, as the most important interaction energy (n-ε_{σ^*}) related to the resonance in the molecule, is found to be relatively high, (LP2 $O_5 \rightarrow \pi^* C_5C_6$) = 47.55 kcal mol^{-1}. This energy amount indicates the hyperconjugation between the electron donating oxygen and the A phenyl ring. The intramolecular hyperconjugative interactions are formed by the orbital overlap between π(C—C) and π^*(C—C) bond orbitals, which results in an intramolecular charge transfer (ICT) causing stabilization of the system. These interactions are observed as an increase in electron density (ED) in C—C anti-bonding orbital that weakens their respective bonds [47]. The ED at the conjugated π and π^* bonds (~1.7e) of the phenyl ring clearly demonstrate strong delocalization of electron leading to the stabilization of morin structure by the amount of ~30–45 kcal mol^{-1}. A very strong interaction has been observed between the π type orbital containing the lone electron pair of all OH groups, and neighboring anti-bonding orbitals of the benzene rings. This interaction, as one responsible for a pronounced decrease of the lone pair orbital occupancy compared to other occupancy, points to the hyperconjugation between the oxygen atoms and the benzene ring. These ICT results support the facts of so far known bioactivity of morin. The natural Mulliken population analysis of morin was calculated also using the M05-2X/6-311++G(d,p) level. The natural charge distribution structure of morin is shown in Fig. 1b. As expected, the negative charge is distributed almost uniformly over oxygen atoms of all OH groups, although, it should be noted that the O3 and O2′ are slightly more negative than others which may indicate them as positions through which morin undergoes chemical reactions more easily.

The most stable structure of morin indicates strongly localized double bonds at the C2—C3 and C4—O positions of the ring C. The bond order values suggest a highly independent electronic delocalization in the rings B and A, which is also one of the main structural features implicated in antioxidant activity of flavon-3-ols. The C2—C1′ bond lies in the chromone plane, because the torsional angle τ is 168.8° and its length is 1.464 Å. The bond order of the C2—C1′ bond obtained by the NBO analysis is close to 1 while its length is 1.464 Å. Both these values indicate that there is very small conjugation across all the rings of the π system. The positions of the double bonds in the ring C around the carbonyl group indicate a crossconjugated system [48] in which the delocalization is allowed only between C and A or C and B rings but not between the rings A and B. This fact is indirectly confirmed by the investigation in which biphenol molecules were found to be neither completely planar nor conjugated [48].

3.3. Analysis of IR and Raman spectra

Vibrational normal mode assignments for morin are done on the basis of a best-fit comparison between the experimentally obtained and theoretically calculated spectra. The experimentally obtained, theoretically calculated and scaled band positions, wavenumbers, along with the corresponding assignments for the first 69 vibrational modes (of total 90) appearing in the 3700–500 cm^{-1} region, are listed in Table 2. Table 2 also lists relative descriptions of IR and Raman intensities, potential energy distribution (PED) values and the description of the largest vibrational contributions to the normal modes.

The most distinct and easily recognizable broad bands in IR spectrum of morin and polyphenols generally (also alcohols when analyzed) are the bands in high frequency region (4000–2000 cm^{-1}) assigned to different modes of O—H vibrations (Table 2). This region of morin IR spectrum is dominated by very massive and intense overlapping bands (Fig. 3a). Taking into account the polyhydroxylated structure of morin molecule the intense bands, positioned at 3565 (ν_{90}), 3508 (ν_{89}), 3384 (ν_{88}) and 3311 (ν_{87}) and 3244 cm^{-1} (ν_{86}), could be taken as possible, different, absorptions for hydrogen bonds in morin. This is also the result confirmed by theoretical calculations which predict

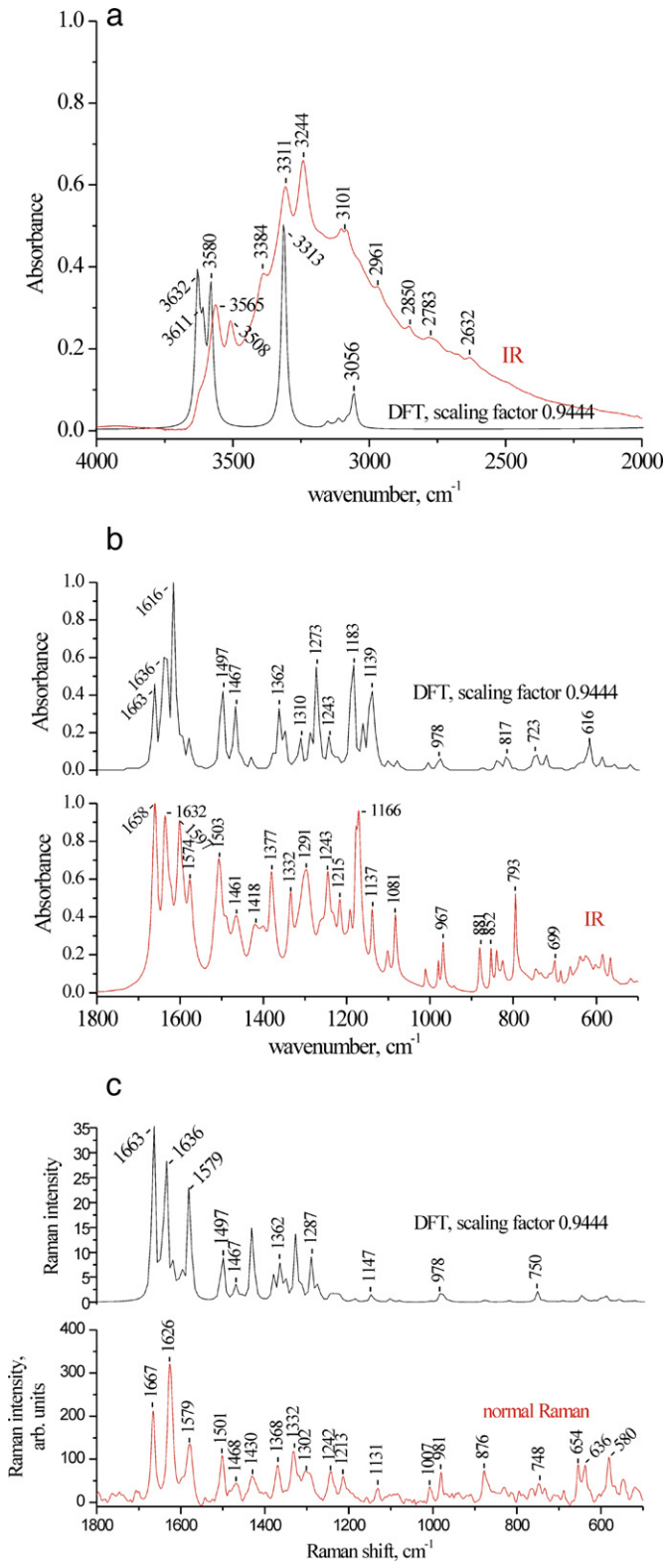

Fig. 3. Different wavenumber regions of experimentally obtained and theoretically calculated IR* (a and b) and Raman (c) spectra of morin. *IR spectra are normalized to 1.0 absorbance scale value.

hydrogen bonding (Table 1). Some degree of discrepancy between DFT calculated and experimentally obtained wavenumber values could be taken as the consequence of possible molecular interactions or as a consequence of DFT calculations performed for the gas phase.

The high frequency region, is also very characteristic to various C—H stretching modes.

From Fig. 3a it is evident that between 3100 and 2630 cm^{-1} there are several shoulders which could be assigned to different C—H stretching modes. The vibrational contributions to the normal stretching modes (PED values) (Table 2) in the 3700–3000 cm^{-1} region are assigned solely to the O—H and C—H stretching modes themselves (99–100%) while the rest of the modes are presented as the combination of various contributions.

The low frequency (1800–500 cm^{-1}) regions of IR and normal Raman spectra of morin powder are shown in Fig. 3b and c along with the theoretically calculated spectra. The DFT wavenumbers are adjusted by a uniform scaling factor of 0.9444 [30–33] in order to obtain the best fit of the observed data. As Fig. 3b and c shows the DFT calculated band positions provide very good fit to the experimental values in the high wavenumber region. Below 1100 cm^{-1} the number of bands in DFT calculated spectrum is much lower and the match is not so accurate. The bands in this region could be combination or overtone bands or even some impurity in the sample from other substances or maybe even polymerization. The predicted DFT band intensities also do not coincide with the experimental values especially in the low frequency region.

The majority of the intense bands both in IR and Raman spectra are to be found in the 1800–1500 cm^{-1} wavenumber region. As in the other flavone derivatives [49–53] this region involves a combination of the C=O stretching ($1632_{(IR)}$ and $1574_{(IR)}$ cm^{-1}; $1626_{(R)}$ and 1579_{R} cm^{-1}) (modes ν_{79} and ν_{76}), C2=C3 stretching ($1658_{(IR)}$ and $1632_{(IR)}$ cm^{-1}; $1667_{(R)}$ and $1626_{(R)}$ cm^{-1}) (ν_{80} and ν_{79}) and C—C stretching ($1658_{(IR)}$, $1632_{(IR)}$, $1597_{(IR)}$ and $1574_{(IR)}$ cm^{-1}; $1667_{(R)}$, $1626_{(R)}$ and $1579_{(R)}$ cm^{-1}) modes (ν_{80}–ν_{76}) (Table 2, Fig. 3b and c). As the result of increased conjugation of the carbonyl group with the pyrone ring through the C2=C3 bond [48,49] the frequencies of the most intense bands, assigned to both the C=O and C2=C3 stretching modes (ν_{79} and ν_{80}), are little bit decreased and positioned at lower values compared to flavanone (1695 cm^{-1}), flavone (1649 cm^{-1}), and 5—OH flavone (1657 cm^{-1}) [49,50].

The bands between 1500 and 1000 cm^{-1} (ν_{74}–ν_{51}) mostly involve C—C stretching, O—C stretching and in-plane C—C—H, C—O—H, C—C—O and C—C—C bending vibrations of the rings. The most intense bands in this region of the IR spectrum belong to modes ν_{74}, ν_{69}, ν_{67}, ν_{65}, ν_{63}, and ν_{59} and in Raman spectrum to modes ν_{74}, ν_{69}, ν_{67}, ν_{66}, ν_{63} and ν_{61} (Fig. 3b and c).

Bands appearing below 1000 cm^{-1}, medium to low intensity, are assigned to bending modes (C—C—O, C—C—C, C—O—H, H—C—C and C—O—C) of all three rings and also to the combination of various in plane (C—C—C—H, H—C—C—H, C—C—C—C, C—C—O—C) and out of plane (O—C—C—C and C—C—O—C) modes.

3.4. Comparative analysis of the spectra

The assignment of the most prominent normal modes in Raman spectrum of morin is qualitatively verified through comparative spectral analysis with quercetin (2-(3,4-dihydroxyphenyl)-3,5,7-trihydroxy-4H-chromen-4-one) (Fig. S1). Quercetin has been one of the most extensively studied flavones owing to its specific chemical structure and unique properties. Morin and quercetin are structural isomers differing only in the structure of the B ring (C3′—OH, C4′—OH in quercetin and C2′—OH, C4′—OH in morin) which makes the comparison of the spectra easily obtainable and descriptive enough. The O—H and C—H stretching region (3700–3000 cm^{-1}) is not analyzed because of the lack of the bands in the Raman spectrum. The 1800–500 cm^{-1} region, as the most prominent one, is analyzed and compared (Fig. 4). The matching bands are labeled with asterisks. Experimental and calculated positions of the bands in the Raman spectrum of quercetin are listed in Table S2.

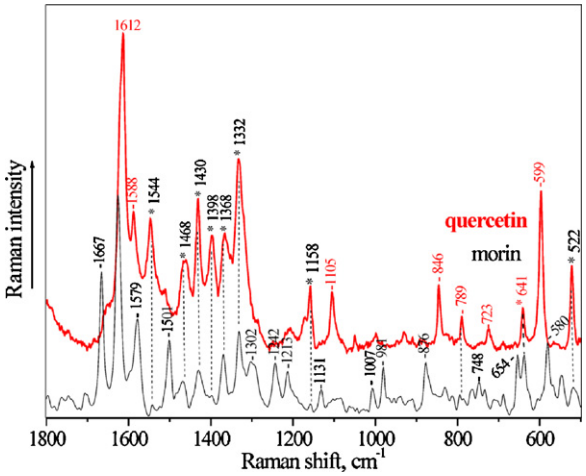

Fig. 4. 1800–500 cm^{-1} Raman regions of quercetin (upper trace) and morin (down trace) spectra. The matching bands are labeled with asterisk.

The most prominent bands in morin spectrum are assigned to C—C stretching (C2=C3), O—C stretching (C3—O, C5—O) and carbonyl stretching (C=O) (ν_{80}, ν_{79} and ν_{76}) modes at 1667, 1626 and 1579 cm^{-1}, respectively (Fig. 4). This region resembles the most intense lines in the corresponding spectrum of quercetin and its C3- and C5-hydroxy derivatives as well [50]. In the spectrum of quercetin those vibrations are assigned to the modes ν_{80}, ν_{78}, ν_{76}, respectively (Table S2). It is evident that the bands at 1667 and 1626 cm^{-1} in the spectrum of morin are somewhat shifted toward higher wavenumbers while the band at 1579 cm^{-1} is shifted to lower wavenumbers (Fig. 4).

The matching bands labeled with asterisks in Fig. 4 point to the structural features which are common to both morin and quercetin structures (Figs. 1 and S1). Those bands are at 1544 cm^{-1} (ν_{75}) (assigned to C=O stretching and C5—O stretching modes), 1468 (ν_{72}) and 1398 (ν_{70}) cm^{-1} (C3—O, C5—O and C7—O stretching), 1430 cm^{-1} (ν_{71}) (C3—OH and C5—OH bending), 1368 cm^{-1} (ν_{69}) (C4′—OH bending), 1332 cm^{-1} (ν_{67}) (C3—OH bending), 1158 cm^{-1} (ν_{58}) (C4′—OH bending). All those structural features, carbonyl group at position C4, hydroxyl groups at C3, C5, C7 and C4′, are common to both molecules.

The discriminant bands in the spectrum of morin (Fig. 4) point to the structural features by which morin and quercetin differ. Those bands are: 1501 cm^{-1} (ν_{74}) (assign C2′—C3′—C4′ and H3′—C3′—C4′ bending modes of the ring B), 1302 cm^{-1} and 1242 cm^{-1} (ν_{66} and ν_{63}) (both assigned to C2′—OH and C4′—OH bending modes), 1213 cm^{-1} (ν_{61}) (C2′—O, C3—O and C5—O stretching), 1131 cm^{-1} (ν_{56}) (C2′—OH bending), 981 cm^{-1} (ν_{50}) (C2′—C3′—C4′ and H5′—C5′—C4′ bending), 876 cm^{-1} (ν_{47}) (H3′—C3′—C2′ bending mode), 765 cm^{-1} (ν_{43}) (C2′—C1′—C6′ bending), 748 cm^{-1} (ν_{42}) (C3′—C4′—C5′ bending) 735 cm^{-1} (ν_{41}) (C2′—C3′—C4′ bending) 654 cm^{-1} (ν_{36}) (C—C—O bendings of the ring B) and 580 cm^{-1} (ν_{30}) (C—C—C bendings of the rings C–B).

In quercetin spectrum discriminant bands are positioned at: 1105 cm^{-1} (ν_{54}) (C3′—OH bending), 846 cm^{-1} (ν_{47}) (H2′—C3′—C4′ bending), 723 cm^{-1} (ν_{42}) (C3′—C4′—O4′ C3′—C4′—C5′ bending), 599 cm^{-1} (ν_{34}) (C3′—C4′—O4′ and C2′—C3′—O3′ bending) and 723 cm^{-1} (n_{42}) (C3′—C4′—O4′ and C3′—C4′—C5′ bending). It is evident (Table 2) that all listed bands solely assign different bending modes of the ring B. The arguments gained through the comparative analysis of the spectra undoubtedly point to the difference in the B ring hydroxylation pattern.

4. Conclusions

The obtained results demonstrate the applicability and performance of DFT calculations to give a conformational analysis of morin at the state of isolated molecule. The DFT calculations are proven as an accurate source of normal mode assignments since they quite acceptably reproduce the main characteristics of the experimental morin spectrum. This further could provide good insight into the structural changes which appear upon all relevant interactions of not only morin but also other structurally similar flavone molecules.

Acknowledgements

The authors acknowledge financial support by the Ministry of Science of Republic of Serbia (Grant No. 172015 and Serbia–Croatia Bilateral agreement 2011–2012). The authors thank Prof. Jamróz MH for VEDA 4 programme.

Appendix A. Supplementary data

Supplementary data associated with this article can be found, in the online version, at http://dx.doi.org/10.1016/j.vibspec.2012.10.006.

References

[1] W.R. Markesbery, M.A. Lovell, Antioxidants Redox Signal. 8 (2006) 2039–2045.
[2] B. Halliwell, Drugs Aging 18 (2001) 685–716.
[3] W.R. Markesbery, Free Radic. Biol. Med. 23 (1997) 134–147.
[4] W.R. Markesbery, Brain Pathol. 9 (1999) 133–146.
[5] B. Drew, C. Leeuwenburgh, Ann. N.Y. Acad. Sci. 959 (2002) 66–81.
[6] X. Huang, Mutat. Res. 533 (2003) 153–171.
[7] N.D. Hajiliadis (Ed.), Cytotoxic, Mutagenic, and Carcinogenic Potential of Heavy Metals Related to Human Environment, Kluwer Academic Press, Netherlands, 1997.
[8] M. Vokurkova, S. Xu, R.M. Touyz, Future Cardiol. 3 (2007) 53–63.
[9] D. Steinberg, J. Biol. Chem. 272 (1997) 20963–20966.
[10] T. Ide, H. Tsutsui, S. Hayashidani, D. Kang, N. Suematsu, K. Nakamura, Circ. Res. 88 (2001) 529–535.
[11] J.B. Harborne, Comparative Biochemistry of the Flavonoids, Academic Press, London/New York, 1967.
[12] G. Di Carlo, N. Mascolo, A.A. Izzo, F. Capasso, Life Sci. 65 (4) (1999) 337–353.
[13] J.B. Harborne, Plant Flavonoids in Biology and Medicine. 11: Biochemical, Cellular and Medicinal Properties, Alan R. Liss, New York, 1988, pp. 17–27.
[14] V. Cody, E. Middleton, J.B. Harborne, Plant flavonoids in Biology and Medicine – Biochemical Pharmacological and Structure–Activity Relationships, Alan R. Liss, New York, 1986, pp. 429–440.
[15] N.P. Das, Flavonoids in Biology and Medicine III—Current Issues in Flavonoids Research, Singapore University Press, Singapore, 1990.
[16] A. Mora, M. Paya, J.L. Rios, M.J. Alearaz, Biochem. Pharmacol. 40 (4) (1990) 793–797.
[17] S.H. Fang, Y.C. Hou, W.C. Chang, S.L. Hsiu, P.D. Chao, B.L. Chiang., Life Sci. 74 (2003) 743–756.
[18] J. Brown, J. O'Prey, P.R. Harrison, Carcinogenesis 24 (2003) 171–177.
[19] W. Krol, S. Dworniczak, G. Pietsz, Z.P. Czuba, M. Kunicka, M. Kopacz, D. Nowak, Acta Pol. Pharm. 59 (2002) 77–79.
[20] F.O. Ranelletti, R. Ricci, L.M. Larocca, N. Maggiano, A. Capelli, Int. J. Cancer 50 (1992) 486–492.
[21] P. Thuillier, A.R. Brash, J.P. Kehrer, J.B. Stimmel, L.M. Leesnitzer, P. Yang, R.A. Newman, S.M. Fischer, Biochem. J. 366 (2002) 901–910.
[22] A.K. Ratty, J. Sunamoto, N.P. Das, Biochem. Pharmacol. 37 (1988) 989–995.
[23] T. Ikegawa, H. Ohtani, N. Koyabu, T. Nakamura, T. Uchiumi, M. Kuwano, H. Ohtani, Y. Sawada, Cancer Lett. 177 (2002) 89–93.
[24] M.K. Shukla, M. Dubey, E. Zakar, R. Namburu, Z. Czyznikowska, J. Leszczynski, Chem. Phys. Lett. 480 (2009) 269–272.
[25] Y. Zhao, D.G. Truhlar, Theor. Chem. Acc. 120 (2008) 215–241.
[26] M.J. Frisch, G.W. Trucks, H.B. Schlegel, G.E. Scuseria, M.A. Robb, J.R. Cheeseman, V.G. Zakrzewski, J.A. Montgomery Jr., R.E. Stratmann, J.C. Burant, S. Dapprich, J.M. Millam, A.D. Daniels, K.N. Kudin, M.C. Strain, O. Farkas, J. Tomasi, V. Barone, M. Cossi, R. Cammi, B. Mennucci, C. Pomelli, C. Adamo, S. Clifford, J. Ochterski, G.A. Petersson, P.Y. Ayala, Q. Cui, K. Morokuma, A.D. Malick, K.D. Rabuck, K. Raghavachari, J.B. Foresman, J. Cioslowski, J.V. Ortiz, A.G. Baboul, B.B. Stefanov, G. Liu, A. Liashenko, P. Piskorz, I. Komaromi, R. Gomperts, R.L. Martin, D.J. Fox, T. Keith, M.A. Al-Laham, C.Y. Peng, A. Nanayakkara, M. Challacombe, P.M.W. Gill, B. Johnson, W. Chen, M.W. Wong, J.L. Andres, C. Gonzalez, M. Head-Gordon, E.S. Replogle, J.A. Pople, Gaussian 09, Revision A.1-SMP, Gaussian Inc., Wallingford, CT, 2009.

[27] Y. Zhao, N.E. Schultz, D.G. Truhlar, J. Chem. Phys. 123 (2005), 161103(1–5).
[28] Y. Zhao, N.E. Schultz, D.G. Truhlar, J. Chem. Theory Comput. 2 (2006) 364–382.
[29] M.H. Jamróz, Vibrational Energy Distribution Analysis, VEDA 4, Warsaw, 2004.
[30] M.W. Wong, Chem. Phys. Lett. 256 (1996) 391–399, 454.
[31] J.P. Merrick, D. Moran, L. Radom, J. Phys. Chem. A 111 (2007) 11683–11700.
[32] K.J. Jalkanen, P.J. Stephens, J. Phys. Chem. 95 (1991) 5446–5454.
[33] A.E. Reed, R.B. Weinstock, F. Weinhold, J. Chem. Phys. 83 (1985) 735–746.
[34] J.E. Carpenter, F. Weinhold, J. Mol. Struct. Theochem. 46 (1988) 41–62.
[35] E.D. Glendening, A.E. Reed, J.E. Carpenter, Weinhold F NBO Version 3.1.
[36] A.E. Reed, L.A. Curtiss, F. Weinhold, Chem. Rev. 88 (1988) 899–926.
[37] R. Wysokinsk, K. Hernik, R. Szostak, D. Michalska, Chem. Phys. 333 (2007) 37–48.
[38] V. Cody, J.R. Luft, J. Mol. Struct. 317 (1–2) (1994) 89–97.
[39] S. Marković, S.V. Mentus, J.M. Dimitrić Marković, J. Phys. Chem. A 113 (2009) 14170–14179.
[40] P. Foster, F. Weinhold, J. Am. Chem. Soc. 102 (1980) 7211–7218.
[41] F. Weinhold, C.R. Landis, Valency and Bonding: A Natural Bond Orbital Donor–Acceptor Perspective, Cambridge University Press, New York, 2005.
[42] W. Thomson, P. Torkington, J. Chem. Soc. (1945) 640–644.
[43] N. Liu, Z.R. Chen, S.F. Yuan, J. Zhejiang Univ. Sci. B 6 (2005) 584–589.
[44] J. Chocholousová, V. Spirko, P. Hobza, PCCP 6 (2004) 37–41.
[45] D. Glendening, J.K. Badenhoop, A.E. Reed, J.E. Carpenter, J.A. Bohmann, C.M. Morales, F. Weinhold, NBO 5.9, Theoretical Chemistry Institute, University of Wisconsin, Madison, 2001.
[46] C. James, A. Amal Raj, O.F. Nielson, V.S. Jayakumar, I. Hubert Joe, Spectrochim. Acta 70A (2008) 1208–1246.
[47] B. Smith, Infrared Spectral Interpretation: A Systematic Approach, CRC Press, Washington, DC, 1999.
[48] W. Hutter, H.K. Bodenseh, J. Mol. Struct. 291 (1993) 151–158.
[49] Z. Jurasekova, J.V. Garcia-Ramos, C. Domingo, S. Sanchez-Cortes, J. Raman Spectrosc. 37 (2006) 1239–1241.
[50] T. Teslova, C. Corredor, R. Livingstone, T. Spataru, R.L. Birke, J.R. Lombardi, M.V. Cañamares, M. Leona, J. Raman Spectrosc. 38 (2007) 802–818.
[51] Z. Jurasekova, A. Torreggiani, M. Tamba, S. Sanchez-Cortes, J.V. Garcia-Ramos, J. Mol. Struct. 918 (2009) 129–137.
[52] A. Torreggiani, A. Trinchero, M. Tamba, P. Taddei, J. Raman Spectrosc. 36 (2005) 380–388.
[53] A. Torreggiani, Z. Jurasekova, S. Sanchez-Cortes, M. Tamba, J. Raman Spectrosc. 39 (2008) 265–275.